Wave power extraction from a multi-OWC platform

Siming Zheng, Alessandro Antonini, Yongliang Zhang, Jon Miles, Gregorio Iglesias

Abstract—**In this paper, a rectangular barge consisting of multiple oscillating water columns (OWCs) is considered, hereinafter referred to as a multi-OWC platform. Each OWC chamber is enclosed by two vertical side walls with its bottom submerged and open to the sea. As ocean waves propagate through the multi-OWC platform, the water column enclosed in each chamber rises and falls, causing an oscillating air pressure inside the chamber and driving the air to flow through a turbine installed at the chamber top. An analytical model based on linear potential flow theory and eigen-function expansion method is developed to solve the wave diffraction and radiation problems from the multi-OWC platform with consideration of the effect of both the thickness and the draft of the walls of the OWC chambers. Assuming the effect of the turbine as a linear power take-off (PTO) system, the analytical model is further applied to calculate the motion response, power absorption, and reflection and transmission coefficients of the multi-OWC platform. The effects of the PTO coefficients, the number of constituent chambers, the overall device dimensions and the relative dimensions of adjacent chambers on the power extraction are investigated. A smaller-draft front wall and a larger-draft back wall are found to be beneficial for broadening the range of high efficiency performance of the platform.**

Keywords—**Wave energy, hydrodynamics, analytical model, OWCs, power extraction.**

I. Introduction

OSCILLATING water columns (OWCs) are recognized as one of the most successful wave energy converters due to its structural and mechanical simplicity [1]-[5]. A typical OWC is composed of a fixed hollow structure with its bottom submerged and open to the sea. Subjected to water waves, the water column enclosed by the structure chamber moves up and down, driving the air inside and outside the chamber to flow through a turbine, which in turn drives a generator to produce electricity.

So far, most studies on OWC have been focused on single-chamber OWC devices. Falnes and McIver [6] carried out a numerical study of an offshore single-chamber OWC device, in which the chamber was enclosed by two rigidly connected vertical thin barriers of unequal length oscillating in the surge mode. Its turbine characteristics were assumed linear and it could achieve complete absorption of the incident waves for optimum conditions. A nearshore single-chamber OWC device in constant water depth that consists of a thin vertical surface-piercing barrier in front of a vertical wall was later simulated by Evans and Porter [7] by an analytical model based on 2D potential flow theory. To deal with the singular behaviour in the velocity field at the gap under the thin barrier, a Chebyshev polynomial based integral equation was applied. The analytical results showed that all incident wave power could be captured at resonance conditions. The effect of a stepped bottom topography in increasing the efficiency of such nearshore single-chamber OWC was analytically, numerically and physically investigated by Rezanejad et al. [8], [9] later.

Recently, the concepts of dual-chamber and multi-chamber OWC devices were proposed to improve wave power extraction by broadening the range of high efficiency performance. Rezanejad et al. [10] developed analytical and numerical models for the performance of a nearshore dual-chamber OWC in finite water depth. The draft of the outside chamber was found to be the dominant parameter in determining the basic resonance frequency that contributed to power extraction. Similarly, the performance of the dual-chamber OWC over stepped bottom was analysed [11]. The OWC with the steps on the sea bed was found to have a wide frequency bandwidth in the computed range of wave periods. Numerical and physical studies on dual-chamber OWC can also be found in [12]-[15]. More recently, Noad and Porter [16] presented a simplified analytical study of an offshore multi-chamber OWC. Results demonstrated that varying

ID number 1296 and conference track WHM. This work was supported by Intelligent Community Energy (ICE), INTERREG V FCE, European Commission (Contract No. 5025).

Siming Zheng is with the School of Engineering, University of Plymouth, Drake Circus, Plymouth PL4 8AA, UK (e-mail: siming.zheng@plymouth.ac.uk).

Alessandro Antonini is now at Department of Hydraulic Engineering, Delft University of Technology, The Netherlands.

Yongliang Zhang is with State Key Laboratory of Hydroscience and Engineering, Tsinghua University, Beijing, 100084, China.

Jon Miles is with the School of Engineering, University of Plymouth, Drake Circus, Plymouth PL4 8AA, UK.

Gregorio Iglesias is at MaREI, Environmental Research Institute & School of Engineering, University College Cork, Ireland. He is also with the School of Engineering, University of Plymouth, Drake Circus, Plymouth PL4 8AA, UK.

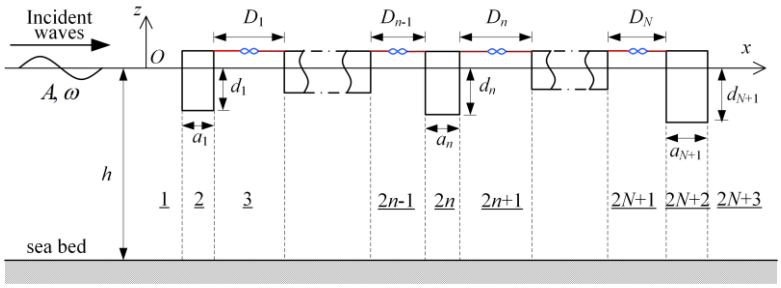

Fig. 1. Side view of the multi-OWC platform.

chamber size lead to a broader-band power absorption efficiency response, and avoided the zeros in power extraction that had been seen for equally-sized chambers. While notably shallow-draft, thin walls and infinite water depth conditions were assumed in their model.

In this paper, a stationary rectangular barge consisting of multiple OWCs is considered, hereinafter referred to as a multi-OWC platform (see Fig. 1). Different from the previous analytical models of OWCs applying either a thin-wall restriction or a shallow draft restriction, in the present work an analytical model of the multi-OWC platform, based on linear potential flow theory and an eigen-function expansion method is developed with neither the thin-wall nor the shallow draft restriction. In other words, the effect of both the thickness and the draft of the walls of the OWC chambers is taken into consideration in the present model. This will enable more details of the properties of the device to be captured.

An advantage of the analytical model is its computational efficiency, which allows sensitivity analysis to be carried out for a large range of device parameters. Specifically, the effects of the PTO coefficients, the number of constituent chambers, the overall device dimensions and the relative dimensions of adjacent chambers (width, thickness and draft of chamber walls) on the power extraction of the multi-OWC platform are investigated.

II. ANALYTICAL MODEL

A. Problem description

As shown in Fig.1, the multi-OWC platform is located at the free-surface of the sea with the water depth h and water density ρ. A Cartesian coordinate $Oxyz$ is adopted with the origin O in the mean water level and Oz pointing vertically upwards. The length of the platform in the y direction is assumed to be far longer than a wave length and there are no intermediate walls along the x direction, so the hydrodynamic problem can be treated as a 2D one. The platform is comprised of a series of N rectangular chambers in x direction, in which the nth chamber is enclosed by the nth and (n+1)th walls in the y direction. The width of the nth chamber is denoted as D_n, and the thickness and draft of the nth wall are represented by a_n and d_n, respectively. As ocean waves propagate through the multi-OWC platform along the Ox-axis, the water column enclosed in each chamber rises and falls, causing an oscillating air pressure inside the chamber and in turn driving the air flow through a turbine installed at the chamber top. In this paper, regular incident waves of a small wave slope are considered, and the amplitude and angular frequency are represented by A and ω, respectively. The chamber air is assumed to be incompressible and the effect of the air turbine in each chamber can be characterized as a linear damping. The damping induced by the turbine in the nth chamber is denoted as c_n.

B. Formulation of the wave diffraction/radiation problem

In common with the assumptions that have been adopted in [17], [18], in this paper, the fluid is considered isotropic and incompressible inviscid, the time-harmonic flow is irrotational, and the deformation and motion of the platform are neglected.

With the employment of a standard linearized theory of water waves, the fluid motion can be expressed by the velocity potential $\varphi=\mathrm{Re}[\Phi(x,z)e^{-i\omega t}]$, where i is the imaginary unit, t is the time. Φ is a complex spatial velocity potential satisfying the Laplace equation, and can be decomposed into an incident wave spatial potential Φ_I, a diffracted wave spatial potential Φ_0 and N radiated wave spatial potential:

$$\Phi=\Phi_I+\Phi_0+\sum_{L=1}^{N}p_L\Phi_L\,, \tag{1}$$

where p_L is the complex air pressure amplitude inside the Lth OWC chamber; Φ_L (L=1, 2, …, N) is the spatial velocity potential due to unit air pressure oscillation inside the Lth OWC chamber.

An expression for Φ_I, the dominating equation, and the boundary conditions that Φ_0 should satisfy, can be found in our previous paper [17]. Here, the governing equation and boundary conditions that Φ_L(L=1, 2, …, N) should satisfy are given as follows.

$$\partial^2\Phi_L/\partial x^2+\partial^2\Phi_L/\partial z^2=0\,, \tag{2}$$

$$\partial\Phi_L/\partial z-\omega^2\Phi_L/g=\delta_{L,n}\mathrm{i}\omega/(\rho g)\,,\ (z=0,\ x<x_{l,1},\ x_{r,n}<x<x_{l,n+1},\ x>x_{r,N+1}), \tag{3}$$

$$\partial\Phi_L/\partial z=0\,,\ (z=-h), \tag{4}$$

$$\partial \Phi_L / \partial z = -\delta_{L,0}\, \partial \Phi_I / \partial z, \ (z=-d_n,\ x_{l,n}<x<x_{r,n}), \tag{5}$$

$$\partial \Phi_L / \partial x = -\delta_{L,0}\, \partial \Phi_I / \partial x, \ (-d_n<z<0,\ x=x_{l,n},\ x=x_{r,n}), \tag{6}$$

$$\Phi_L \text{ outgoing; finite value, } (|x|=\infty), \tag{7}$$

in which $x_{l,n}$ and $x_{r,n}$ denote the positions of the left and right edges of the nth wall in Ox-axis; $\delta_{L,0}$ denotes the Kronecker delta; g is the acceleration due to gravity.

C. Solution to diffracted/radiated potentials

To solve the wave diffraction and radiation problems, the fluid domain is divided into $2N+3$ subdomains denoted as Ω_n (n=1, 2, …, $2N$+3) as shown in Fig. 1. Utilizing the method of separation of variables, the analytical expressions for unknown Φ_L (L=0, 1, 2, …, N) in each subdomain, i.e., regions 1, $2n$+1, $2n$ and $2N$+3, can be expressed as follows [17]-[19]:

$$\Phi_1^{(L)} = \sum_{j=1}^{\infty} A_{1,j}^{(L)} \mathrm{e}^{\lambda_j x} Z_j(z) \ \text{ in } \Omega_1, \tag{8}$$

$$\Phi_{2n+1}^{(L)} = \sum_{j=1}^{\infty} \left(A_{2n+1,j}^{(L)} \mathrm{e}^{\lambda_j x} + B_{2n+1,j}^{(L)} \mathrm{e}^{-\lambda_j x} \right) Z_j(z) - \frac{\mathrm{i}\delta_{L,n}}{\rho\omega} \text{ in } \Omega_{2n+1}, \tag{9}$$

$$\Phi_{2n}^{(L)} = -\delta_{L,0}\Phi_I + A_{2n,1}^{(L)} x + B_{2n,1}^{(L)} + \sum_{j=2}^{\infty} \left(A_{2n,j}^{(L)} \mathrm{e}^{\beta_{n,j} x} + B_{2n,j}^{(L)} \mathrm{e}^{-\beta_{n,j} x} \right) \cos\left[\beta_{n,j} (z+h) \right] \text{ in } \Omega_{2n}, \tag{10}$$

$$\Phi_{2N+3}^{(L)} = \sum_{j=1}^{\infty} A_{2N+3,j}^{(L)} \mathrm{e}^{-\lambda_j x} Z_j(z) \ \text{ in } \Omega_{2N+3}, \tag{11}$$

in which $A_{1,j}^{(L)}$, $A_{2n+1,j}^{(L)}$, $B_{2n+1,j}^{(L)}$, $A_{2n,j}^{(L)}$, $B_{2n,j}^{(L)}$, and $A_{2N+3,j}^{(L)}$ are unknown coefficients to be determined; $\beta_{n,j}$ and λ_j are the eigenvalues of the j-th wave modes in subdomain $2n$, and other subdomains, and Z_j is an eigenfunction as:

$$\lambda_1 = -\mathrm{i}k, \ j=1, \tag{12}$$

$$\omega^2 = -\lambda_j g \tan(\lambda_j h), \ j=2, 3, 4, \ldots, \tag{13}$$

$$\beta_{n,j} = (j-1)\pi/(h-d_n), \ j=2, 3, 4, \ldots, \tag{14}$$

$$Z_j(z) = N_j^{-0.5} \cos\left[\lambda_j (h+z) \right], \ N_j = \frac{1}{2}\left[1 + \frac{\sin(2\lambda_j h)}{2\lambda_j h} \right]. \tag{15}$$

where k is the wave number satisfying $\omega^2=gk\tanh(kh)$.

The continuity conditions of pressures or/and normal velocities at the interfaces between any two adjacent subdomains that should be satisfied by Φ_L (L=0, 1, 2, …, N) are presented as follows:

$$\frac{\partial \Phi_{2n-1}^{(L)}}{\partial x} = \begin{cases} -\delta_{L,0}\, \partial \Phi_I / \partial x, & \left(x = x_{L,n}, \ -d_n < z < 0 \right) \\ \partial \Phi_{2n}^{(L)} / \partial x, & \left(x = x_{L,n}, \ -h < z < -d_n \right) \end{cases}, \tag{16}$$

$$\frac{\partial \Phi_{2n+1}^{(L)}}{\partial x} = \begin{cases} -\delta_{L,0}\, \partial \Phi_I / \partial x, & \left(x = x_{R,n}, \ -d_n < z < 0 \right) \\ \partial \Phi_{2n}^{(L)} / \partial x, & \left(x = x_{R,n}, \ -h < z < -d_n \right) \end{cases}, \tag{17}$$

$$\Phi_{2n-1}^{(L)} = \Phi_{2n}^{(L)}, \quad \left(x = x_{L,n}, \ -h < z < -d_n \right), \tag{18}$$

$$\Phi_{2n}^{(L)} = \Phi_{2n+1}^{(L)}, \quad \left(x = x_{R,n}, \ -h < z < -d_n \right). \tag{19}$$

Upon substituting (8–11) for Φ_L in different subdomains into these continuity conditions (16-19), utilizing the orthogonality relations of the integration of eigen-functions over the vertical dimension and taking the first M terms in the infinite series, a linear system of $4(N+1)M$ complex equations for each Φ_L with the same number of unknown coefficients are obtained. The unknown coefficients can be easily evaluated by solving a $4(N+1)M$ -order linear matrix equation [17], [18].

D. Hydrodynamic coefficients due to wave diffraction and radiation

1) Direct Method (DM) for solving hydrodynamic coefficients

The upward flux at the water surface inside the nth OWC chamber due to the contributions of undisturbed incident wave and the diffracted wave, the so-called excitation volume flow, can be written as Re[$F_e^{(n)} \mathrm{e}^{-\mathrm{i}\omega t}$],

$$F_e^{(n)} = \int_{x_{r,n}}^{x_{l,n+1}} \partial\left(\Phi_I + \Phi_0 \right) / \partial z \big|_{z=0} \, \mathrm{d}x. \tag{20}$$

The complex amplitude of the upward flux at the water surface inside the nth OWC chamber due to the radiated waves induced by the oscillations of the OWC chambers can be written as

$$\begin{aligned} F_R^{(n)} &= \int_{x_{R,n}}^{x_{L,n+1}} \partial \sum_{L=1}^{N} p_L \Phi_L \Big/ \partial z \big|_{z=0} \, \mathrm{d}x \\ &= \frac{\omega^2}{g} \sum_{L=1}^{N} p_L \sum_{j=1}^{\infty} \left[A_{2n+1,j}^{(L)} \left(\mathrm{e}^{\lambda_j x_{L,n+1}} - \mathrm{e}^{\lambda_j x_{R,n}} \right) - B_{2n+1,j}^{(L)} \left(\mathrm{e}^{-\lambda_j x_{L,n+1}} - \mathrm{e}^{-\lambda_j x_{R,n}} \right) \right] \frac{Z_j(0)}{\lambda_j} \\ &= \sum_{L=1}^{N} p_L \left(\mathrm{i} a_{n,L} - c_{n,L} \right) \end{aligned}, \tag{21}$$

where $a_{n,L}$ and $c_{n,L}$ are the so-called radiation susceptance and radiation conductance, respectively,

$$a_{n,L}=\frac{\omega^2}{g}\mathrm{Im}\left(\sum_{j=1}^{\infty}\left[A_{2n+1,j}^{(L)}\left(\mathrm{e}^{\lambda_j x_{\mathrm{L},n+1}}-\mathrm{e}^{\lambda_j x_{\mathrm{R},n}}\right)-B_{2n+1,j}^{(L)}\left(\mathrm{e}^{-\lambda_j x_{\mathrm{L},n+1}}-\mathrm{e}^{-\lambda_j x_{\mathrm{R},n}}\right)\right]Z_j(0)/\lambda_j\right), \quad (22)$$

$$c_{n,L}=-\frac{\omega^2}{g}\mathrm{Re}\left(\sum_{j=1}^{\infty}\left[A_{2n+1,j}^{(L)}\left(\mathrm{e}^{\lambda_j x_{\mathrm{L},n+1}}-\mathrm{e}^{\lambda_j x_{\mathrm{R},n}}\right)-B_{2n+1,j}^{(L)}\left(\mathrm{e}^{-\lambda_j x_{\mathrm{L},n+1}}-\mathrm{e}^{-\lambda_j x_{\mathrm{R},n}}\right)\right]Z_j(0)/\lambda_j\right). \quad (23)$$

2) Indirect method for solving hydrodynamic coefficients

Apart from using the direct method, the excitation volume flow may also be expressed in terms of the radiated wave's far-field coefficients using the Haskind Relation (HR) as:

$$F_{\mathrm{e}}^{(n)}=2\mathrm{i}\rho gAkhA_{1,1}^{(n)}/Z_1(0). \quad (24)$$

Similarly, with the employment of the Haskind Relation (HR), $c_{n,L}$ can be written in terms of the radiated wave's far-field coefficients as follows

$$c_{n,L}=\omega\rho kh\left(A_{2N+3,1}^{(n)*}A_{2N+3,1}^{(L)}+A_{1,1}^{(n)*}A_{1,1}^{(L)}\right). \quad (25)$$

where the superscript * denotes complex-conjugate.

E. Power absorption

After solving the wave diffraction/radiation problem and obtaining the hydrodynamic coefficients, the water column motion response of the multi-OWC platform in frequency domain can be calculated by the equation:

$$\left[-\mathrm{i}\mathbf{M}_{\mathrm{a}}+\left(\mathbf{C}_{\mathrm{d}}+\mathbf{C}_{\mathrm{PTO}}\right)\right]\dot{\boldsymbol{X}}=\boldsymbol{F}_{\mathrm{e}} \quad (26)$$

where $\mathbf{M}_{\mathrm{a}}$ and $\mathbf{C}_{\mathrm{d}}$ are the matrices of $a_{n,L}$ and $c_{n,L}$, respectively; $\mathbf{C}_{\mathrm{PTO}}$ denotes a diagonal damping matrix induced by the power take-off (PTO) system (i.e., turbines) [20]; $\dot{\boldsymbol{X}}=[p_1\ p_2\ \ldots\ p_N]^{\mathrm{T}}$ is the air pressure response vector of the multi-OWC chamber to be determined; $\boldsymbol{F}_{\mathrm{e}}$ is the wave excitation volume flux vector.

The time averaged wave power absorbed by the platform can be evaluated by

$$P=\frac{1}{2}\sum_{n=1}^{N}c_n|p_n|^2. \quad (27)$$

The power absorption efficiency is defined as

$$\eta=P/\left(0.5\rho gA^2c_g\right), \quad (28)$$

where the denominator denotes the incident wave power, in which c_g represents the wave group velocity.

F. Wave reflection and transmission coefficients

The wave reflection coefficient and the wave transmission coefficient of the multi-OWC platform, denoted as R and T, respectively, can be calculated as:

$$R=\left|\frac{\omega}{gA}Z_0(0)\left(A_{1,1}^{(0)}+\sum_{n=1}^{N}p_nA_{1,1}^{(n)}\right)\right|, \quad (29)$$

$$T=\left|1+\frac{\mathrm{i}\omega}{gA}Z_0(0)\left(A_{2N+3,1}^{(0)}+\sum_{n=1}^{N}p_nA_{2N+3,1}^{(n)}\right)\right|. \quad (30)$$

III. Model Validation

To validate the analytical model for solving wave diffraction/radiation problems as described in Section II, wave excitation volume flux and hydrodynamic coefficients are evaluated by using both the direct method and indirect method. Figure 2 presents the comparison

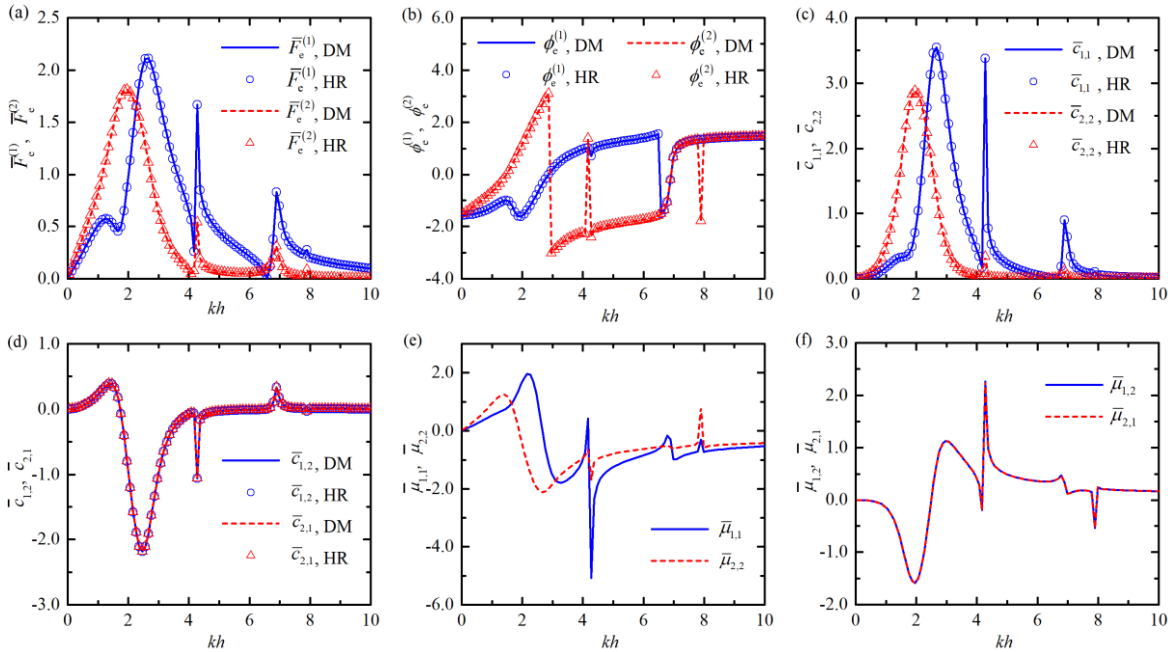

Fig. 2. Wave excitation volume flux and hydrodynamic coefficients for N=2, h=10 m, a_1/h=a_2/h=a_3/h=0.05, D_1/h=0.5, D_2/h=0.8, d_1/h=0.1, d_2/h=0.2, d_3/h=0.3, $x_{1,1}$=0.0: (a) $\bar{F}_{\mathrm{e}}^{(1)}$ and $\bar{F}_{\mathrm{e}}^{(2)}$; (b) $\phi_{\mathrm{e}}^{(1)}$ and $\phi_{\mathrm{e}}^{(2)}$; (c) $\bar{c}_{1,1}$ and $\bar{c}_{2,2}$; (d) $\bar{c}_{1,2}$ and $\bar{c}_{2,1}$; (e) $\bar{\mu}_{1,1}$ and $\bar{\mu}_{2,2}$; (f) $\bar{\mu}_{1,2}$ and $\bar{\mu}_{2,1}$.

between these results for N=2, h=10 m, $a_1/h=a_2/h=a_3/h$=0.05, D_1/h=0.5, D_2/h=0.8, d_1/h=0.1, d_2/h=0.2, d_3/h=0.3, in which the physical quantities have been nondimensionalized by

$$\bar{F}_e^{(j)}=\frac{\left|F_e^{(j)}\right|}{A\sqrt{gh}},\ \left\{\bar{c}_{i,j},\bar{\mu}_{i,j},\bar{c}_{\mathrm{opt}}^{(j)}\right\}=\frac{\rho g}{\sqrt{gh}}\left\{c_{i,j},\mu_{i,j},c_{\mathrm{opt}}^{(j)}\right\},\ \bar{p}_j=\frac{p_j}{\rho gA}. \quad (31)$$

Additionally, the results of η, R, T and $\eta+R^2+T^2$ for the same platform with $\mathbf{C}_{\mathrm{PTO}}=diag(\mathbf{C}_d)$ is illustrated in Fig.3.

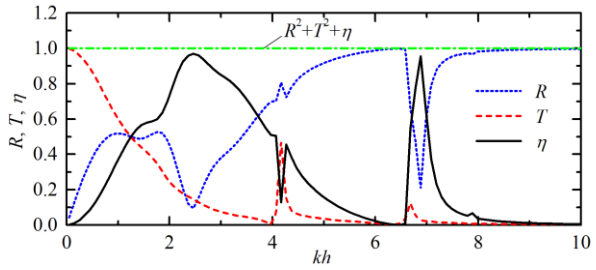

Fig. 3. Wave reflection and transmission coefficients and wave power absorption efficiency for N=2, h=10 m, $a_1/h=a_2/h=a_3/h$=0.05, D_1/h=0.5, D_2/h=0.8, d_1/h=0.1, d_2/h=0.2, d_3/h=0.3, $\mathbf{C}_{\mathrm{PTO}}=diag(\mathbf{C}_d)$.

Figures 2 and 3 show that the results of wave excitation volume flux and hydrodynamic coefficients by using two different methods are in excellent agreement and the energy conservation relationship, i.e., $\eta+R^2+T^2=1$, is satisfied perfectly, which validates the present analytical model.

IV. RESULTS AND DISCUSSION

The performance of the multi-OWC chamber platform in terms of wave power extraction depends upon several parameters: the PTO damping coefficients, the width of each chamber, the wall thickness and the draft of each wall, and the number of chambers. Hereinafter, the walls and chambers of the platform are assumed identical, i.e., $a_j=a_n$, $d_j=d_n$ and $D_j=D_n$, unless otherwise specified. The overall length of the platform in the x direction is denoted as l_0, i.e., $l_0=x_{r,N+1}-x_{1,1}$. The effect of multiple parameters on wave power extraction is examined in this section.

G. Effect of PTO damping

Following [21], three PTO strategies are considered, i.e., $\mathbf{C}_{\mathrm{PTO}}=diag(\mathbf{C}_d)$, $\mathbf{C}_{\mathrm{PTO}}=diag((\mathbf{C}_d^2+\mathbf{M}_a^2)^{0.5})$, $\mathbf{C}_{\mathrm{PTO}}=\mathbf{C}_{\mathrm{opt}}$, in which $\mathbf{C}_{\mathrm{opt}}$ represents a diagonal matrix with all elements non-negative that maximize power absorption of the multi-OWC platform.

Figure 4 presents the power absorption efficiency of the platform with these three different PTO strategies for

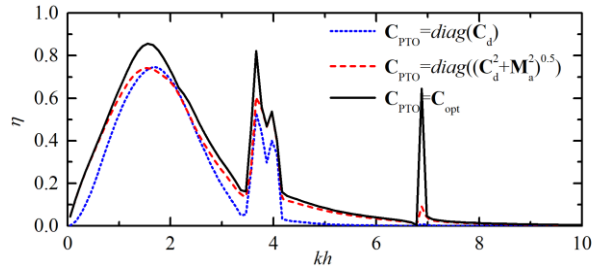

Fig. 4. Wave power absorption efficiency with different PTO strategy for N=2, h=10 m, l_0/h=2.0, a_j/h=0.05, d_j/h=0.2.

N=2, h=10 m, l_0/h=2.0, a_j/h=0.05, d_j/h=0.2. There is a main peak of the η-kh curve and it occurs around kh=1.6 regardless of the PTO strategy adopted. The peak values corresponding to the three PTO strategies are 0.75, 0.74 and 0.86, respectively. The other peaks are observed at higher wave frequencies, i.e., kh=3.8 and 6.9. Note at kh=6.8, there is almost no power absorption. As expected, the corresponding η for Strategy 3 is found to be no less than that of any other two PTO strategies for all range of the computed wave conditions. Although the main peak value of η for Strategy 2 is slightly smaller than that for Strategy 1, performance of the platform with Strategy 2 are much closer to the optimized one (i.e., with Strategy 3) for the rest of wave conditions.

For N=2, the $\mathbf{C}_{\mathrm{opt}}$ adopted in Strategy 3 can be obtained by using an analytical method [18], and for more constituent chambers, i.e., N=3, 4, …, $\mathbf{C}_{\mathrm{opt}}$ can be found by applying numerical iterations which might be much time consuming and/or lead to inaccurate results. Hereinafter, Strategy 2, i.e., $\mathbf{C}_{\mathrm{PTO}}=diag((\mathbf{C}_d^2+\mathbf{M}_a^2)^{0.5})$, which is more straightforward than the Strategy 3 and meanwhile gives better power absorption for most wave conditions than Strategy 1, is employed.

H. Effect of the number of constituent chambers

Figure 5 presents the frequency response of the power absorption efficiency of the multi-OWC platform (h=10 m, l_0/h=2.0, a_j/h=0.05, d_j/h=0.2) with different number of constituent chambers. Since the overall length and thickness of each wall are both fixed, more number of the constituent chambers leads to smaller width of each OWC chamber.

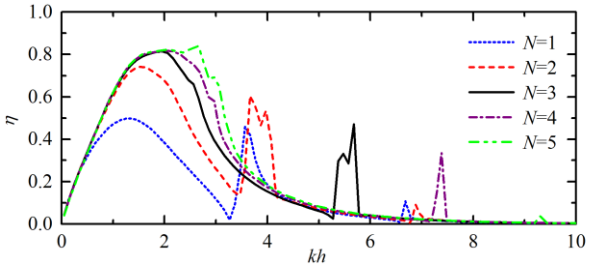

Fig. 5. Wave power absorption efficiency of the platform with different number of constituent chambers, i.e., N, and h=10 m, l_0/h=2.0, a_j/h=0.05, d_j/h=0.2.

As the platform changes from the single-OWC one to the dual-OWC one (i.e., from N=1 to N=2, see Fig. 5), wave power extraction of the platform is significantly improved in terms of both a larger peak value and a larger bandwidth of the main η-kh peak. As N keeps increasing towards N=5, power extraction can be further improved whereas the improvement turns weaker and weaker. For long waves, e.g., kh<0.5, η is found to be independent on N. This is due to the reason that the piston-like motion of the water column dominates all along the platform in long waves and introduction of intermediate walls does not matter. As N increases, all the peaks shift towards larger wave frequencies as illustrated in Fig. 5, and this is induced by the larger resonance frequencies for the smaller-width OWC chambers.

Applying more constituent chambers could obviously enhance power capture ability of the multi-OWC platform. However, it requires more PTO units and more internal walls, which in turn results in higher costs of construction and maintenance. N=2, 3 might be the best option in practice with the trade-off between the power extraction and costs.

I. *Effect of the overall platform length*

Figure 6 illustrates the frequency response of the wave power absorption efficiency of the multi-OWC platform with different overall length for N=2, h=10 m, a_j/h=0.05 and d_j/h=0.2. For the platform consisting of 2 chambers with the size of each wall fixed, increasing the overall platform length is achieved by broadening width of each OWC chamber.

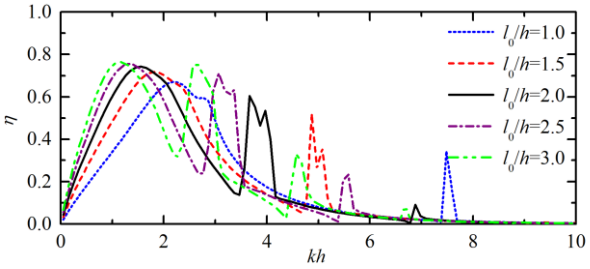

Fig. 6. Wave power absorption efficiency of the platform with different overall platform length, i.e., l_0/h, and N=2, h=10 m, a_j/h= 0.05, d_j/h=0.2.

As illustrated in Fig. 6, the peaks of the η-kh curve shift towards the smaller wave frequencies with the increase of l_0/h. This is reasonable from the view of compatibility between incident wave length and OWC chamber width. More specifically, the OWC chamber with a larger width (i.e., larger l_0/h) is more likely to reach the resonance in longer waves (i.e., smaller kh). Note the peak values of η increase with l_0/h; meanwhile, the two kh values corresponding to the first two peaks are closer together, making the platform more sensitive to wave conditions. In the computed range of wave conditions, there are four peaks observed for l_0/h=3.0, while only three or even two are found for l_0/h=1.0, 1.5, 2.0, and 2.5.

J. *Effect of the wall thickness*

Effect of the wall thickness (i.e., a_j) on power extraction is studied by examining the performance of the platform with the employment of a_j/h= 0.01, 0.03, 0.05, 0.07, 0.09 for N=2, h=10 m, l_0/h=2.0, d_j/h=0.2. Results for these five cases are illustrated in Fig. 7. The main peak of the η-kh curve is found to be slightly weakened in terms of both peak value and bandwidth with the increase of a_j/h. The kh where the main peak occurs seems to be independent on a_j/h. The other peaks at high wave frequencies are found rather sensitive to the change of a_j/h. The larger the value of a_j/h, the narrower and smaller of these peaks, and the larger of the kh where these peaks occur.

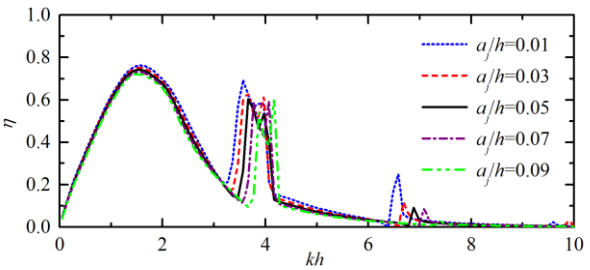

Fig. 7. Wave power absorption efficiency of the platform with different wall thickness, i.e., a_j/h, and N=2, h=10 m, l_0/h=2.0, d_j/h=0.2.

K. *Effect of the wall draft*

Most wave power is concentrated at no more than a fourth wavelength below the sea water level, hence the wall draft of the platform is one of the key factors affecting its power extraction. Figure 8 shows wave power absorption efficiency of the platform with five different values of d_j/h and N=2, h=10 m, l_0/h=2.0, a_j/h=0.05.

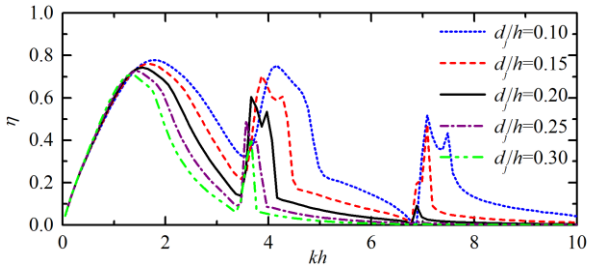

Fig. 8. Wave power absorption efficiency of the platform with different wall draft, i.e., d_j/h, and N=2, h=10 m, l_0/h=2.0, a_j/h=0.05.

Clearly, as plotted in Fig. 8, smaller d_j/h leads to higher and broader peaks of the η-kh curves. The kh values corresponding to these peaks also shift towards larger wave frequencies. While the effect of the wall draft can be neglected for long waves, e.g., kh<1.0. For kh=6.8, no power can be absorbed regardless of the value of d_j/h.

Note in practice, d_j/h cannot be too small for keeping the platform bottom opening submerged all the time in strong waves and/or large tidal range.

L. *Effect of the width ratio of adjacent chambers*

For each case examined in the above subsections (i.e., IV. A-E), the multi-OWC platform is composed of the OWC chambers in same size. In this subsection, the platform consisting of two OWC chambers with unequal width (specifically, D_1/D_2=1/3, 1/2, 1/1, 2/1, 3/1) while the overall platform length fixed is considered. Analytical results of the power absorption efficiency for these cases with five different values of D_1/D_2 are given in Fig. 9, in which results of the single-chamber platform without the intermediate wall are also plotted as a comparison.

Existence of the intermediate wall in the platform is

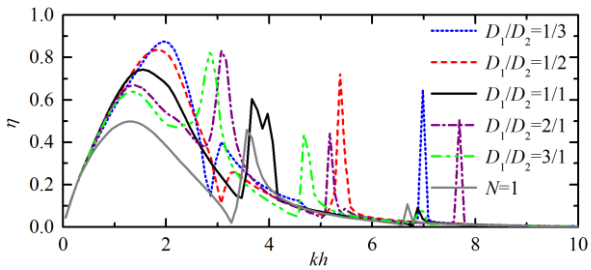

Fig. 9. Wave power absorption efficiency of the platform with different width ratio of adjacent chambers, i.e., D_1/D_2, and N=2, h=10 m, l_0/h=2.0, a_j/h=0.05, d_j/h=0.2.

found to affect power absorption of the platform significantly, especially the main peak in terms of peak values and the kh where the main peak occurs. For N=1, the main peak value of η and the corresponding kh are (0.50, 1.36), whereas for N=2 with D_1/D_2=1/3, 1/2, 1/1, 2/1, 3/1, they are (0.88, 1.96), (0.84, 1.86), (0.74, 1.56) and (0.67, 1.36) and (0.64, 1.36), respectively. As the intermediate wall comes close to the leeward edge of the platform (i.e., a larger value of D_1/D_2), the results are close to the single-chamber results. It is interesting to note that although the largest main peak value (i.e., 0.88) is achieved at kh=1.96 when D_1/D_2=1/3, η drops to merely 0.15 at kh=2.86, where, on the contrary, the η for D_1/D_2=3/1 rises rapidly to the second peak with the value (η=0.84) even larger than its main peak value (η=0.64 at kh=1.36). Similar circumstances also happen for the comparison between the cases of D_1/D_2=1/2 and D_1/D_2=2/1 at kh=3.07. Hence for real sea states, when wave power is concentrated in a small range of wave frequencies, e.g., most of incident wave power exists at 1.0<kh<2.0, the platform with a smaller value of D_1/D_2 is welcome for a better power absorption; while if the incident wave power is distributed in a large range of wave frequencies, e.g., 1.0<kh<3.0, or even for bimodal wave spectra, the platform with its larger OWC chamber placed in the front might be beneficial for power extraction.

M. Effect of the draft ratio of adjacent walls

Finally, we consider the effect of changing the draft ratio of adjacent walls. For the five cases with different d_1/d_2 (specifically, d_1/d_2=1/3, 1/2, 1/1, 2/1, 3/1) studied in this subsection, d_1/d_2=d_2/d_3 and d_2/h=0.2 are satisfied all the time. Results of the wave power absorption efficiency of these cases are illustrated in Fig 10.

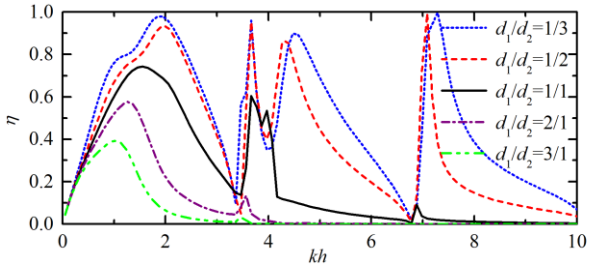

Fig. 10. Wave power absorption efficiency of the platform with different draft ratio of adjacent walls, i.e., d_1/d_2=d_2/d_3, and N=2, h=10 m, l_0/h=2.0, a_j/h=0.05, d_2/h=0.2.

It can be learnt from Fig. 10 that d_1/d_2 plays a dominant role in affecting performance of the platform in capturing wave power. For most wave conditions in the computed range of kh, especially for 0.5<kh<3.0, 4.5<kh<6.5, and 7.4<kh<10.0, as d_1/d_2 increases from 1/3 to 3/1, the η decreases dramatically. For some specified cases, almost all the incident power can be absorbed at specified wave conditions, e.g., d_1/d_2=1/3 and kh=1.86 and 7.29. For d_1/d_2=2/1 or 3/1, η≈0.0 is obtained for kh>4.0. This is reasonable for most wave power is concentrated near the sea water level, and if d_1/h (or d_1/d_2 in this subsection) is large enough or the wave length is small enough, all incident waves can be reflected from the front wall of the platform back to the sea, leading to no power absorption. For d_1/d_2 with a rather small value, e.g., d_1/d_2=1/3, compared to the cases with d_1/d_2≥1/1, on the one hand, incident waves are more easily to enter the OWC chambers of the platform due to a smaller d_1; on the other hand, more power can be reflected from the back wall (less power can be transmitted through the back wall) due to a larger d_2, leading to a significant enhancement of wave power extraction.

Note that η≈0.0 occurs at kh=6.78 regardless of the value of d_1/d_2. Another interesting result that deserves mentioning may be inferred from the comparison between the results of d_1/d_2=1/3 and d_1/d_2=3/1. The main peak for d_1/d_2=3/1 occurs at kh=1.06. For d_1/d_2=1/3, although the main peak happens at kh=1.86, the power extraction can be strengthened as well at kh=1.06 that relevant to the main peak for d_1/d_2=3/1. Similar results can also be observed when comparing the results for d_1/d_2=1/2 and 2/1. It means that adopting a smaller-draft front wall and a larger-draft back wall is beneficial for broadening the range of high efficiency performance of the platform.

V. CONCLUSIONS

A multi-OWC integrated offshore stationary platform, which can work not only as a breakwater to attenuate water waves, but also as a wave energy converter to extract wave power is proposed in this paper. To assess the wave power extraction from such multi-OWC platform, an analytical approach is developed based on linear potential flow theory and eigen-function expansion method. Neither the thin-wall nor the shallow draft restriction is applied in the model, hence it allows us to explore more properties of the platform that cannot be done ever before by the other simplified models. Wave excitation volume flux of each OWC and hydrodynamic coefficients are evaluated based on the diffracted and radiated velocity potentials, respectively. Additionally, an indirect method based on the Haskind Relation is adopted to calculate certain hydrodynamic coefficients, the comparison of which with those obtained from the direct method are used to validate the correctness of the analytical model.

Assuming the effect of the turbine as a linear power take-off (PTO) system, the analytical model is further applied to calculate the motion response, power absorption, and reflection and transmission coefficients of the multi-OWC platform. The energy conservation relationship is also checked to indirectly validate the present analytical model.

The validated analytical model is then applied to investigate the effects of the PTO coefficients, the number of constituent chambers, the overall device dimensions and the relative dimensions of adjacent chambers on the power extraction of the multi-OWC platform. The following conclusions may be drawn.

Performance of the platform with Strategy 2 (i.e., $\mathbf{C}_{PTO}=diag((\mathbf{C}_d^2+\mathbf{M}_a^2)^{0.5})$) are much closer to the optimized one (i.e., Strategy 3) for the computed range of wave conditions, expect the kh where the main peak of η occurs.

As N increases, wave power extraction of the platform is improved in terms of both a larger peak value and a larger bandwidth of the main η-kh peak, and all the peaks of the η-kh curves shift towards larger wave frequencies.

The peaks of the η-kh curve shift towards the smaller wave frequencies and the peak values increase with the increase of the platform overall length (l_0/h). Meanwhile, the two kh corresponding to the first two peaks are closer together for a larger l_0/h, making the platform more sensitive to wave conditions.

The peaks of the η-kh curves at high wave frequencies are found sensitive to the change of wall thickness (a_j/h). The larger the value of a_j/h, the narrower and smaller of these peaks, and the larger of the kh where these peaks occur.

A smaller wall draft (d_j/h) leads to higher and broader peaks of the η-kh curves. Meanwhile, the kh corresponding to these peaks shift towards larger wave frequencies.

For the platform consisting of two OWC chambers, as the intermediate wall of comes close to the leeward edge of the platform, the results of η are close to the single-chamber results.

Adopting a smaller-draft front wall and a larger-draft back wall is beneficial for broadening the range of high efficiency performance of the platform.

The conclusions obtained from the present analytical study are beneficial to design a multi-OWC wave energy converter, or an offshore breakwater consisting of multiple OWCs.

The analytical model developed in this paper can be further extended to study the performance of a floating multi-OWC platform. The viscous effects which induce vortex shedding at the lips of the walls together with the compressibility of the air inside the chambers of the platform are neglected. These effects should be considered in order to obtain more realistic prediction of the platform's performance.

REFERENCES

[1] W. Sheng, "Motion and performance of BBDB OWC wave energy converters: I, hydrodynamics," *Renewable Energy*, vol. 138, pp. 106-120, 2019.

[2] F. He, J. Leng, X. Zhao, "An experimental investigation into the wave power extraction of a floating box-type breakwater with dual pneumatic chambers," *Applied Ocean Research*, vol. 67, pp. 21-30, 2017.

[3] B. Pereiras, I. López, F. Castro, G. Iglesias, "Non-dimensional analysis for matching an impulse turbine to an OWC (oscillating water column) with an optimum energy transfer," *Energy*, vol. 87, pp. 481-489, 2015.

[4] S. Zheng, Y. Zhang, G. Iglesias, "Coast/breakwater-integrated OWC: A theoretical model," *Marine Structures*, vol. 66, pp. 121-135, 2019.

[5] F. He, H. Zhang, J. Zhao, S. Zheng, G. Iglesias, "Hydrodynamic performance of a pile-supported OWC breakwater: An analytical study," *Applied Ocean Research*, 2019. doi: 10.1016/j.apor.2019.03.022

[6] J. Falnes, P. McIver, "Surface wave interactions with systems of oscillating bodies and pressure distributions," *Applied Ocean Research*, vol. 7, no. 4, pp. 225–234, 1985.

[7] D. Evans, R. Porter, "Hydrodynamic characteristics of an oscillating water column device," *Applied Ocean Research*, vol. 17, no. 3, pp. 155–164, 1995.

[8] K. Rezanejad, J. Bhattacharjee, C. Guedes Soares, "Stepped sea bottom effects on the efficiency of nearshore oscillating water column device," *Ocean Engineering*, vol. 70, pp. 25-38, 2013.

[9] K. Rezanejad, J. Bhattacharjee, C. Guedes Soares, "Analytical and numerical study of nearshore multiple oscillating water columns," *Journal of Offshore Mechanics and Arctic Engineering*, vol. 138, 021901, 2016.

[10] K. Rezanejad, C. Guedes Soares, I. López, R. Carballo, "Experimental and numerical investigation of the hydrodynamic performance of an oscillating water column wave energy converter," *Renewable Energy*, vol. 106, pp. 1-16, 2017.

[11] K. Rezanejad, J. Bhattacharjee, C. Guedes Soares, "Analytical and numerical study of dual-chamber oscillating water columns on stepped bottom," *Renewable Energy*, vol. 75, pp. 272-282, 2015.

[12] A. Elhanafi, G. Macfarlane, D. Ning, "Hydrodynamic performance of single-chamber and dual-chamber offshore-stationary oscillating water column devices using CFD," *Applied Energy*, vol. 228, pp. 82-96, 2018.

[13] D. Ning, R. Wang, C. Zhang, "Numerical simulation of a dual-chamber oscillating water column wave energy converter," *Sustainability*, vol. 9, no. 9, 1599, 2017.

[14] D. Z. Ning, R. Q. Wang, L. F. Chen, K. Sun, "Experimental investigation of a land-based dual-chamber OWC wave energy converter," *Renewable and Sustainable Energy Reviews*, vol. 105, pp. 48–60, 2019.

[15] F. He, Z. Huang, A. W. K. Law, "An experimental study of a floating breakwater with asymmetric pneumatic chambers for wave energy extraction," *Applied Energy*, vol. 106, pp. 222–231, 2013.

[16] I. Noad, R. Porter, "Wave energy absorption by a shallow-draughted rectangular barge of oscillating water columns," in *12th European Wave and Tidal Energy Conference*, 27th Aug- 1st Sept 2017, Cork, Ireland.

[17] S. Zheng, Y. Zhang, "Wave diffraction and radiation by multiple rectangular floaters," *Journal of Hydraulic Research*, vol. 54, pp. 102–115, 2016.

[18] S. Zheng, Y. Zhang, "Analytical study on wave power extraction from a hybrid wave energy converter," *Ocean Engineering*, vol. 165, pp. 252–263, 2018.

[19] J. Falnes, Ocean Waves and Oscillating Systems: Linear Interactions Including Wave-Energy Extraction. Cambridge: Cambridge University Press, 2002.

[20] A. J. N. A. Sarmento, A. F. de O. Falcão, "Wave generation by an oscillating surface-pressure and its application in wave-energy extraction," *Journal of Fluid Mechanics*, vol. 150, pp. 467–485, 1985.

[21] S. Bellew, T. Stallard, P. K. Stansby, "Optimisation of a heterogeneous array of heaving bodies," in *8th European Wave and Tidal Energy Conference*, 7th -10st Sept 2009, Uppsala, Sweden.